Bulletin of Earthquake Engineering (2026) 24:1787–1817
https://doi.org/10.1007/s10518-025-02347-y

ORIGINAL ARTICLE

Development of predictive expressions for drift-based damage states for precast columns in socket foundations

Halil Dinçer[1,3] · **Sadık Can Girgin**[2]

Received: 17 May 2025 / Accepted: 5 December 2025 / Published online: 23 December 2025
© The Author(s), under exclusive licence to Springer Nature B.V. 2025

Abstract

Precast concrete structures are composed of columns that exhibit significant flexural behavior, high aspect ratios, and substantial deformation and drift capacities. The existing experimental and analytical expressions found in the literature regarding the deformation and displacement capacities of columns are generally inadequate and not directly applicable to precast columns. Therefore, a comprehensive investigation into the damage capacities of precast columns is necessary. In this study, simplified expressions were developed to estimate drift ratios corresponding to various damage states of square precast columns. The effects of several design parameters, including square section depth, aspect ratio, axial load ratio, reinforcement ratios, material strengths, and embedment depth, on the damage behavior of socket columns were evaluated. Initially, based on existing experimental studies on socket foundations, a simplified equation was proposed to estimate the rotational stiffness of the socket column-foundation connection. Then, a parametric study was conducted, and to generate sufficient data, different column models were created using information obtained from previous studies on precast structures, and pushover analyses were performed. The primary damage states considered in these analyses included reinforcement yielding, concrete cover spalling, longitudinal bar buckling, and concrete crushing. Based on the analysis results, polynomial regression analyses were used to develop simplified expressions to estimate drift ratios. These expressions were found to predict experimentally measured drift values with satisfactory accuracy. Among the evaluated design parameters, the aspect ratio was found to significantly affect drift demands. Additionally, fragility analyses indicated that as the aspect ratio increases, socket columns require larger embedment depths to mitigate damage states related to longitudinal reinforcement yielding and cover concrete spalling.

Keywords Rotational stiffness · Damage states · Precast columns · Embedment depths · Aspect ratio · Socket foundation

Extended author information available on the last page of the article

1 Introduction

Precast reinforced concrete structures are increasingly preferred due to their significant advantages, low cost, high quality, and rapid production (Ertaş 2005; Polat 2010). With the growth of the construction sector and the rising demand for engineered buildings, using precast structures has become more prevalent and essential. A significant portion of industrial structures consists of single-story or partially mid-rise, long-span precast buildings, where columns are connected at the roof level with hinged roof beams. Precast buildings' overall performance and structural integrity primarily depend on the connections between various structural elements. Common connection types include column-to-foundation connections, where columns are rigidly fixed to the foundation to provide rotational stiffness, and beam-column connections within the superstructure, which can be either moment-resisting or hinged. Precast column-to-foundation connections should ensure structural stability by effectively transferring vertical and lateral loads from the columns to the ground through the foundation. Reports from recent earthquakes in Türkiye, such as the 1998 Adana-Ceyhan, 1999 Kocaeli, 2011 Van, and the 2023 Kahramanmaraş earthquakes, indicate that damage to industrial buildings was primarily due to deficiencies in connection details. Damage assessments revealed that significant structural failures occurred because of inadequate anchorage and fastening elements, and due to the collapse of roof beams as a result of insufficient bearing lengths. Shear and flexural failures were also observed at column-to-foundation connections. (Adalıer and Aygün 2001; Saatcioglu et al 2001, Özden et al. 2012; Yeşilyurt et al 2021; Arslan et al 2024).

Precast cantilever columns of single-story precast buildings are structural elements characterized by predominantly flexural behavior, with a shear span-to-depth ratio typically exceeding 10 (Fischinger et al 2008; Arslan et al 2024). Experimental studies have demonstrated that precast columns with sufficient connections to foundations possess significant deformation capacities, achieving drift ratios of up to 7–8% (Karadoğan et al. 2013; Palermo et al. 2006; Negro et al 2006). It is essential for the foundation and its components to provide adequate strength and stiffness, even when the columns are experiencing plastic deformation (Metelli et al 2011; Zhang et al 2021; Cheng et al 2021). One commonly used method for precast column-to-foundations, known as the socket connection, involves placing the column into a socket foundation, with the gap between the column and the socket filled with grout to complete the connection (Osanai et al 1996; Canha et al 2009; Han et al 2023; Pul et al 2014). Precast columns in socket foundations are widely applied in industrial structures in countries such as Türkiye and Italy due to their ease of implementation and low sensitivity to workmanship errors (Deyanova et al 2023; Cogurcu and Uzun 2022). The damage mechanisms and deficiencies observed in previous earthquakes for precast columns in socket foundations can be summarized as follows: the damage mechanisms include plastic hinging and crushing at the column base, cracking and localized crushing at the upper edge of the foundation, column separation, and shear failure in column cross-sections, while the observed deficiencies involve inadequate grout application, insufficient confinement reinforcement, inadequate hook lengths, or improper connection details (Adalier and Aydingun 2001; Saatcioglu et al 2001; Özden et al 2012; Yeşilyurt et al 2021; Arslan et al 2024). (Fig. 1a and b).

Experimental studies on rectangular columns in socket foundations generally focused on evaluating the behavior and performance of precast columns and connections with varying

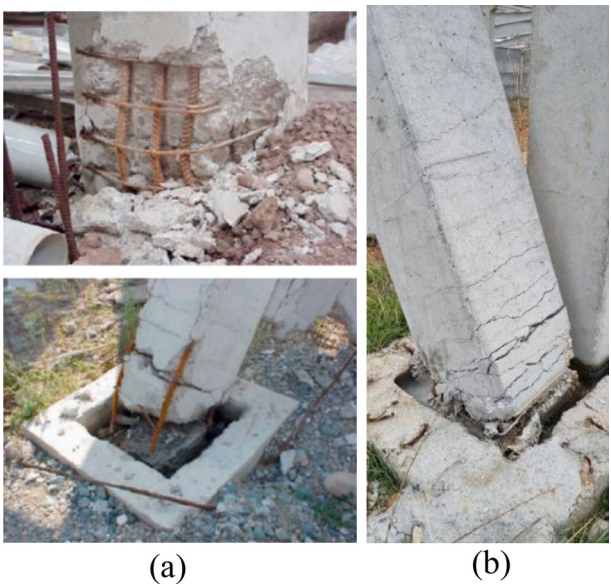

Fig. 1 Typical damages for precast column-to-socket foundations after (**a**) 1999 Kocaeli earthquake (Saatcioglu et al 2001), (**b**) 2023 Kahramanmaraş earthquake

embedment depths and interface conditions. Osanai et al (1996) conducted experimental studies under cyclic loading to investigate the structural behavior of precast column–socket connections. In their study, the force transfer mechanism of columns was modeled considering different embedment lengths and smooth and rough surface conditions. It was concluded that for socket connections with smooth interfaces, an embedment depth of 1.25d (d is the depth of the column cross-section measured in the direction of horizontal loading) was insufficient to achieve adequate stiffness; however, a rigid connection could be achieved when the embedment depth was 1.5d or greater. In contrast, for connections with rough surfaces, an embedment depth of 1.0d or greater was sufficient to provide the required stiffness and force transfer performance for the column. Canha et al (2009 and 2009) investigated precast columns in socket foundations, focusing on the effects of smooth and rough interface conditions, embedment length, and rebar anchorage length. To achieve this, specimens were tested with embedment lengths of 2d and 1.6d, both subjected to significant eccentricity. Their findings indicated that failure occurred outside the embedded region, primarily characterized by the yielding of the tension reinforcement, while the transverse reinforcement exhibited minimal strains. Yüce (2010) and Karadoğan et al (2013) conducted experimental studies on precast columns in socket foundations. Specimens with different cross-sectional dimensions, reinforcement ratios, and interface characteristics in socket foundation connection details were examined. Within the scope of these studies, the behavior and performance of precast columns were comprehensively evaluated in terms of load-displacement hysteretic curves, deformation limits, and failure modes. The experimental results indicated that variations in surface condition (smooth or rough) and embedment depth (1.75d–2.33d) of socket foundation connections had no significant adverse effect on the overall structural behavior of columns.

Pul et al (2014) tested one cast-in-place monolithic connection and five different types of socket foundation connections. It was observed that the standard socket connection with an embedment depth of 0.8d exhibited weaker performance compared to the cast-in-place

column–foundation connection. In addition, innovative materials such as high-performance concrete have been increasingly utilized in precast column connections. For this purpose, Zhang et al (2021) investigated socket connections filled with ultra-high-performance concrete (UHPC). They found that the seismic performance and damage states of precast columns with roughened surfaces and an embedment depth of 0.8d were similar to those of cast-in-place column–foundation connections. The common findings of these studies indicate that in column-to-socket foundation connections, achieving structurally safe and efficient performance requires sufficient embedment depth for the columns.

Although many researchers have developed various equations defining damage limit states for columns in conventional reinforced concrete structures, there are significant uncertainties regarding their direct applicability to precast columns. Kowalsky (2000) recommended damage control deformation limits for circular reinforced concrete bridge columns, and relationships between curvature, drift ratio, ductility, and equivalent viscous damping for columns with different aspect ratios and axial forces were compared, and the variations between them were investigated. Based on plastic hinge analyses, Berry and Eberhard (2003) developed plastic rotation equations at the onset of bar buckling and concrete spalling for flexure-dominated reinforced concrete columns. The equations corresponding to these damage states were calibrated using experimental results obtained from the PEER database (Pacific Earthquake Engineering Research Center) (Berry et al. 2004). Lehman et al (2004) investigated the performance of reinforced concrete bridge columns with varying aspect ratios, axial load ratios, longitudinal and transverse reinforcement ratios. Material strain and displacements corresponding to various damage conditions, such as concrete cracking, cover concrete spalling, core concrete crushing, and reinforcement buckling, were evaluated based on experimental results. Goodnight (2015) developed an experimental program focused on relationships between strain and deformation. Numerical expressions were proposed for the RC bridge columns to assess damage control limit states based on the drift ratio. In recent studies, Shrestha and Pujol (2023) have produced an empirical equation for estimating drifts at a 20% reduction in flexural capacity. The resulting empirical formulation for reinforced concrete columns produced more accurate results than existing formulations in the literature. Aydemir et al (2023) introduced a new model to estimate the drift ratio and displacement capacity of RC columns at the failure damage limit.

Furthermore, studies that predict drift ratios corresponding to damage states for precast columns are limited in the literature. Fischinger et al (2008) developed a modified lumped plastic hinge model to predict the cyclic behavior of precast columns by adapting existing expressions from the literature. However, it was noted that the empirical expressions proposed in the literature for estimating column yielding and ultimate drift capacities (Panagiotakos and Fardis 2001; Fardis and Biskinis 2003; Haselton et al 2008) are not directly applicable for predicting the deformation and displacement capacities of precast columns. The primary reason for this limitation is that these empirical equations were predominantly developed based on experimental databases (PEER database (Berry et al. 2004); Panagiotakos and Fardis 2001) consisting of columns with shear span ratios typically less than 6. In contrast, precast structural elements, which often have larger aspect ratios and slender cross-sections, fall outside the range of these experimental datasets. Deyanova et al (2023) recently evaluated the nonlinear behavior and seismic performance of precast columns using fiber-based nonlinear finite element models. The analysis consists of a simplified analytical method for predicting collapse mechanisms and force–displacement relationships. How-

ever, these studies were based on a limited number of column tests. Therefore, developing simple empirical predictive expressions that use precast columns with different geometric and material properties would be essential for accurately identifying damage levels.

This study aims to develop predictive expressions for various damage states of square-section precast columns in socket foundations based on drift ratios and to propose a simplified equation for evaluating the stiffness of the socket–foundation connection. In this context, the formulation of empirical predictive expressions derived from different geometric and material properties will be crucial for accurately identifying damage levels in precast columns.

2 Predicting rotational stiffness

Embedment depth is one of the critical parameters governing the seismic performance of precast columns in socket foundations and is also important for evaluating potential damage mechanisms during earthquakes. Accurately estimating the behavior and stiffness of precast columns in socket foundations, considering embedment depth, contributes to a reliable assessment of structural performance and improves the accuracy of performance analyses of precast concrete columns. However, a limited number of studies focus on the rotational stiffness of reinforced concrete socket–foundation connections. Han et al (2023) developed a method to estimate the rotational stiffness of precast columns in socket foundations using equations derived from the beam-on-elastic-foundation theory originally established by Hetényi (1946). The validated model showed that reducing embedment length decreased socket connection stiffness. Similarly, Richards et al (2018) and Tryon (2016) studied the estimation of the rotational stiffness of steel column-to-concrete foundation connections, also employing beam-on-elastic-foundation formulas based on Hetényi's theory. Accurate estimation of the rotational stiffness based on these formulas depends on the reasonable determination of the subgrade modulus to be used in the calculations.

Additionally, Barnwell (2015) evaluated expressions for the initial stiffness of the system (k_t) and column stiffness (k_c) using the relationship between springs in series to determine the stiffness of the connection. Han et al (2023) investigated the efficiency of socket connections using the ratio (k_t)/(k_c), defined as the connection efficiency coefficient (α). The finite element analysis conducted by the researchers determined that the parameter with the greatest effect on the connection efficiency coefficient (α) was the embedment depth. These experiments and theoretical studies (Barnwell 2015; Tryon 2016; Richards et al 2018; Han et al 2023) focus on the initial slope of the force-displacement curve at low loading cycles or drift values. They aim to determine the stiffness of the connection before a sudden decrease or change in the initial slope. The initial slope corresponds to the total stiffness at the base of the column. In this study, the total stiffness is determined by employing the stiffness mechanism described in Barnwell (2015). Dividing the lateral load (F) by the displacement (Δ) can give the total or initial stiffness (k_t) of the precast socket column, as given in Eq. (1). F and Δ were determined from the experimental results corresponding to the elastic state of the hysteretic curve. In this study, both values were obtained at the point where cover concrete cracking was first observed in the tests. Once points have been determined, total stiffness, k_t, can be calculated.

$$k_t = \frac{F}{\Delta} \tag{1}$$

Equation (2) provides an alternative expression for stiffness, which can be used to determine the theoretical stiffness of a column with a fixed connection at its base. If the precast column-to-socket connection exhibits deflections smaller than the theoretical displacement given by $FL^3/3EI$, the connection can be considered as a fixed support with sufficiently high rotational stiffness. Here, E is the modulus of elasticity of the concrete column, calculated as $E = 5000\sqrt{f_c}$, I is the moment of inertia of the section, L is the height of the column from the point of load application to the top of the concrete socket.

$$k_c = \frac{3\,EI}{L^3} \tag{2}$$

In this study, a simplified equation is proposed to estimate rotational stiffness at the base of the column-to-socket foundation. The theoretical stiffness of the fixed base column (k_c) and total stiffness (k_t) will be calculated as the first stage of the equation to be derived. The stiffness calculated at low deflection cycles of the force-displacement curve provides important information for finding the rotational stiffness. Experimental studies (Osanai et al 1996; Canha et al 2009; Zhang et al 2021) have shown that the interface conditions, such as smooth or rough between the socket foundation affect the seismic performance of precast columns. In this study, considering the existing experimental results, it was observed that more detailed data can be obtained from studies where the column-foundation connection surface is smooth. Therefore, the data on the initial slope of the hysteresis curve are taken from these experimental studies and evaluated. Table 1 shows the material properties, cross-sectional dimensions, concrete cracking points obtained from cyclic tests, and stiffnesses obtained from references for precast columns with smooth surface socket foundations. This stiffness was taken as the slope of the line drawn from the origin to the concrete cracking, and it was considered as the initial stiffness of the force-displacement curve. EI represents the elastic flexural stiffness of the column, calculated as the product of *E* and the moment of inertia *I*. The parameter (α) was calculated for all test results and is given in the last column of Table 1. The embedded depth ratio (l/d), defined as the ratio of the embedment depth of the socket column specimens to the column depth, varies between 0.6 and 2.33. Also, in Table 1, (b) and (d) indicate the column width and depth, perpendicular and parallel to the horizontal load, respectively.

The equation of connection efficiency developed by Han et al (2023) does not include the case where the embedment depth exceeds 1.2d. For this reason, in this study, the connection efficiency factor α is proposed for a wider range (from 0.6d to 2.3d). To propose an empirical equation, embedment depth was considered a potential predictor variable that influences the performance of the socket column. The empirical equation for α, derived from the optimal fitting solution of the predictive variables, is presented in Eq. (3).

$$\alpha = \frac{k_t}{k_c} = -0.102\left(\frac{l}{d}\right)^2 + 0.626\left(\frac{l}{d}\right) - 0.016 \tag{3}$$

Table 1 Material properties and measured stiffness parameters of the selected references

	No	Reference	ID	Colum size (mm)		fc (MPa)	EI (kNm^2)	l (mm)	l/d	F (kN)	Δ (mm)	k_t (N/m) ($1x10^6$)	k_c (N/m) ($1x10^6$)	α: kt/kc
				b	d									
Test	1	Karadoğan et al (2013)	S30_14	300	300	45.9	22865.47	700	2.33	8	7.7	1.04	1.28	0.81
	2		S30_16	300	300	44.2	22438.04	700	2.33	5.4	4.1	1.32	1.26	1.05
	3		S30_18	300	300	45.8	22840.55	700	2.33	10.1	10	1.01	1.28	0.79
	4		S35_1416	350	350	45.8	42314.93	700	2.00	16	9	1.78	2.37	0.75
	5		S35_18	350	350	45.8	42314.93	700	2.00	14.8	6.6	2.24	2.37	0.95
	6		S35_20	350	350	45.8	42314.93	700	2.00	13	6.1	2.13	2.37	0.90
	7		S40_16	400	400	45.9	72266.17	700	1.75	20.9	6.9	3.03	4.05	0.75
	8		S40_20	400	400	45.9	72266.17	700	1.75	24.2	7.4	3.27	4.05	0.81
	9		S40_2020	400	400	45.9	72266.17	700	1.75	20.8	6.7	3.10	4.05	0.77
Test	10	Osanai et al (1996)	Type 10	400	500	39	130104.1	750	1.50	110	1.5	73.33	115.65	0.63
	11		Type 15	400	500	41	133398.4	750	1.50	70	1	70.00	118.58	0.59
	12		Type 16	400	500	43	136613.3	625	1.25	110	1.5	73.33	121.43	0.60
	13		Type 17	400	500	40	131761.6	500	1.00	110	1.5	73.33	117.12	0.63
Test	14	Canha et al (2009) and Ebeling (2006)	PL_80	400	400	53	96000	800	2.00	40	2.5	16.00	20.18	0.79
Test	15	Cogurcu and Uzun (2022)	SC2	200	300	31	12527	400	1.30	9	0.73	12.33	18.13	0.68
Finite Element Analysis	16	Han et al (2023)	S2-21	670	670	50	473000	402	0.60	*	*	28.8	90.8	0.32
	17		S2-22	670	670	50	487000	469	0.70	*	*	33.9	93.6	0.36
	18		S2-23	670	670	50	496000	536	0.80	*	*	38.8	95.3	0.41
	19		S2-24	670	670	50	501000	603	0.90	*	*	43.8	96.1	0.46
	20		S2-25	670	670	50	506000	670	1.00	*	*	48.6	97.0	0.50
Test	21	Zhang et al (2021)	S2	670	670	50	593708.1	536	0.80	200	4.5	44.4	114.0	0.39

*: Information was not available

This equation provides a reasonable agreement between the predicted and experimental values with low estimation errors. Figure 2 shows the variation of the α factor with respect to the embedment depth ratio. The plotted data show a trend of increasing connection efficiency factor with increasing embedment depth. High l/d ratios (≥2) in some experimental tests indicate that precast socket foundation connections exhibited behavior close to the theoretical fixed-base stiffness and high rotational restraint. Moreover, for specimen S30_16, the observed stiffness exceeding the theoretical fixed-base value may be attributed to factors such as the method used to determine the initial slope, the presence of the grout layer, and friction or stress distribution at the connection interface.

The test results of the α coefficient above were used to estimate the rotational stiffness of the socket column connection. Fig. 3a illustrates the flexural behavior of the socket column under axial and lateral loads, while Fig. 3b schematically shows the relationship between the resulting horizontal displacements and the rotation at the base. In Fig. 3b, the red line on the right represents the deformed shape of the column due to bending, whereas the black line on the left depicts the rigid column prior to bending. Rotational stiffness of the column can be determined by dividing the moment M_{base} by the rotation $\theta_{con.}$ which was obtained using Eq. (4) and represented with β as a rotational spring stiffness, as shown in Fig. 3b. In this equation, deflection ($\Delta_{con.}$) due to the rotation of the connection was obtained by subtracting the part of flexural deformation ($\Delta_{col.}$) from overall deformation ($\Delta_{tot.}$) of the socket column. In previous studies (Han et al 2023; Zhang et al 2021; Karadoğan et al 2013; Osanai et al 1996, the effect of axial forces was taken into account; accordingly, this study considers the effect of axial force on the column-base connection in terms of rotational stiffness. Consequently, the bending moment of the column base M_{base} includes two components: moment multiplying lateral load (F) by column height (L) and additional moment caused by axial loads (N) in combination with column displacement ($\Delta_{tot.}$). The data utilized to compute the ratio $M_{base}/\theta_{con.}$ were mentioned in the previous paragraphs, where the derivation from the linear-elastic stage of load-displacement curves. By solving Eqs. (1, 2, and 4), the corresponding rotational stiffness is derived depending on the α coefficient and given in the following Eq. (5). Finally, a simplified version of the rotational stiffness can be calculated in Eq. (6) by replacing the coefficient α as expressed in Eq. (3).

$$\beta = \frac{M_{base}}{\theta_{con.}} = \frac{FL + N\Delta_{tot.}}{\frac{\Delta_{con.}}{L}} = \frac{FL^2 + N\Delta_{tot.}L}{\Delta_{tot.} - \Delta_{col.}} = \frac{FL^2 + N\Delta_{tot.}L}{\Delta_{tot.} - \frac{FL^3}{3EI}} \tag{4}$$

$$\beta = \frac{M_{base}}{\theta_{con.}} = \frac{L^2 + \frac{NL}{k_c\alpha}}{\frac{1}{k_c\alpha} - \frac{L^3}{3EI}} = \left(\frac{3EI}{L} + NL\right)\frac{\alpha}{(1-\alpha)} \tag{5}$$

$$\beta = \left(\frac{3\,EI}{L} + NL\right)\frac{\left(-0.102\left(\frac{l}{d}\right)^2 + 0.626\left(\frac{l}{d}\right) - 0.016\right)}{\left(+0.102\left(F\frac{l}{d}\right)^2 - 0.626\left(\frac{l}{d}\right) + 1.016\right)} \tag{6}$$

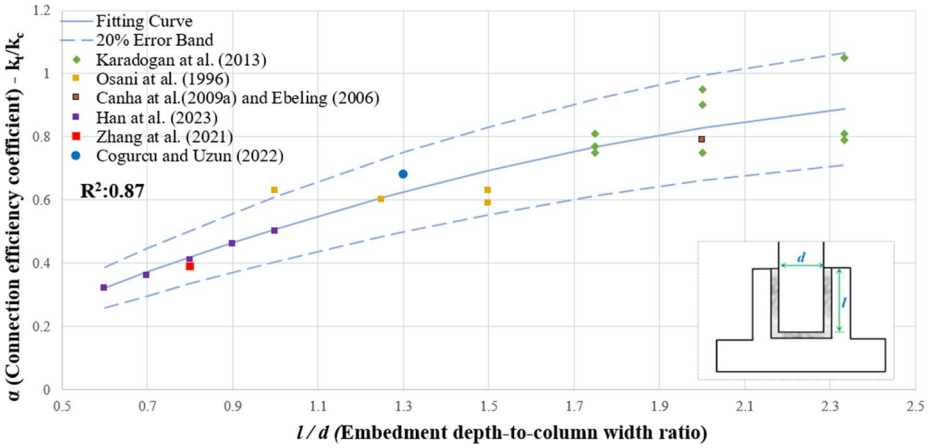

Fig. 2 Connection efficiency coefficient and embedment depth relationship

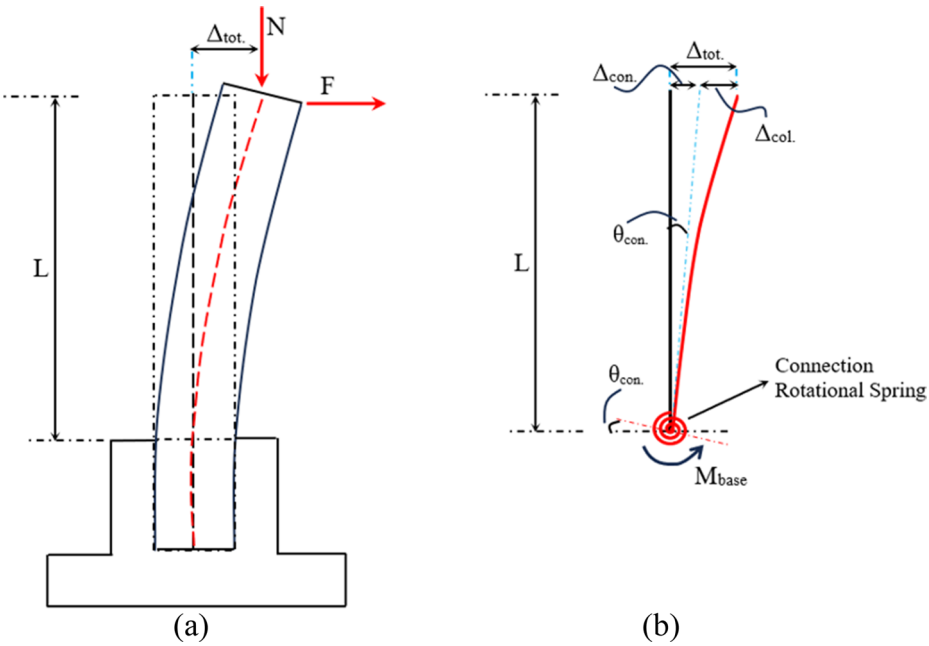

Fig. 3 (**a**) Flexural behaviour and (**b**) rotational flexibility of the column-to-socket foundation

3 Numerical modelling of precast column tests

An experimental research program was carried out at the Structural Engineering Laboratory of Istanbul Technical University (ITU), in collaboration with the Turkish Precast Concrete Association (Yüce 2010; Karadoğan et al 2013). The aim of this study was to evaluate the effectiveness of enhanced detailing and potential improvements in the cyclic performance of

precast columns embedded in socket foundations. Within this scope, precast column specimens were tested, varying in cross-sectional dimensions (30, 35, and 40 cm) and longitudinal and transverse reinforcement ratios. In the cyclic tests, the precast column specimens were subjected to cyclic displacements under a constant axial load with a 4–5% ratio until substantial damage developed. The observed failure modes included concrete cracking at the column base, buckling of the longitudinal reinforcement, and fracture of several longitudinal bars.

In this study, the cyclic behaviors of two precast column specimens, namely S35_1416 and S40_20, were investigated using a numerical model that incorporates foundation stiffness. The corresponding concrete compressive strengths of the columns were 45.8 MPa and 45.9 MPa, respectively, as shown in Table 1 (Karadoğan et al 2013). The simulations were carried out using the OpenSees-based STKO (Scientific Toolkit for OpenSees), developed by Petracca et al (2017), which provides an efficient interface for modeling, visualization, and pre-/post-processing in performance-based earthquake engineering. For the numerical solution, the Krylov-Newton method was employed, and a convergence criterion was applied to control the residual error, maintaining it within a tolerance value of 10^{-6}.

In the structural model, a force-based finite element formulation with distributed plasticity was adopted to accurately capture plastic deformations. Figure 4 illustrates a simplified and representative fiber cross-section used in the analytical model of the column. In this model, the section is discretized into steel, confined concrete, and unconfined concrete fibers, which are distributed along the height of the element at predefined integration points. The strain in each fiber is calculated through sectional analysis, enabling a detailed representation of damage progression within the fiber-based modeling framework.

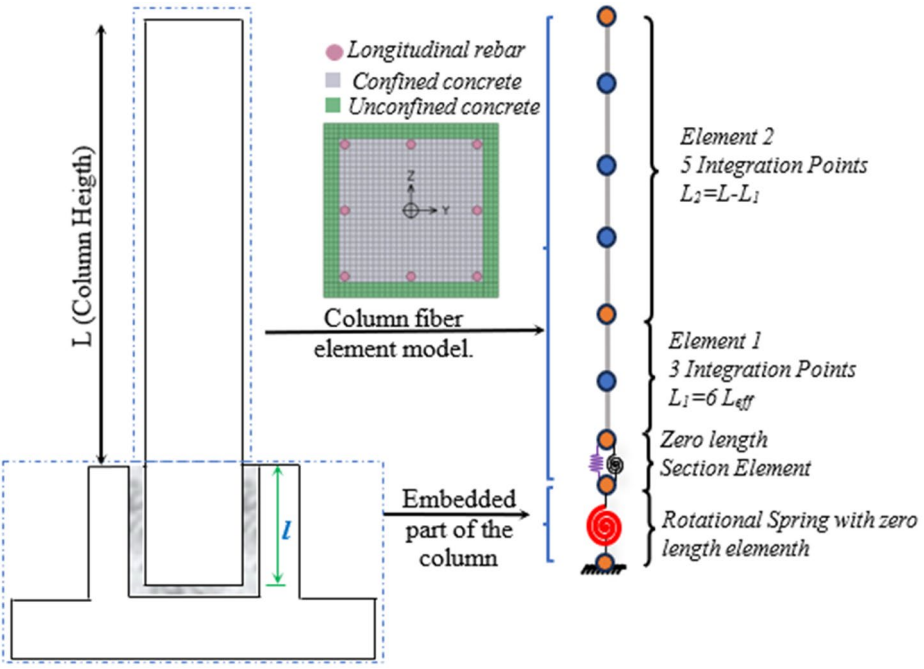

Fig. 4 Numerical model of precast column in socket foundations

For modeling reinforced concrete elements, selecting integration points and the number of elements is critical for accurately predicting the nonlinear response. Thus, in this study, the model proposed by Kashani et al (2016) is used to predict the nonlinear behavior of precast columns in socket foundations. In this proposed model, there are two force-based elements that have different lengths along the column. The first element has three Gauss-Lobatto integration points, where most of the nonlinear deformations are localized, and its total length is $6L_{\text{eff}}$. L_{eff} represents the buckling length of the longitudinal rebar, and the process of determining the buckling length is presented by Dhakal and Maekawa (2002). The second force-based element, which has five integration points, is employed to simulate the upper section of the column based on the suggestion by Berry and Eberhard (2006). Figure 4 illustrates the representation of the proposed model for the precast column in socket foundations.

Fiber sections are assigned nonlinear uniaxial material models to define the monotonic and cyclic response of unconfined and confined concrete and reinforcing steel. In this study, the *Concrete04* material model was selected as the uniaxial material model, available in the OpenSees library. This model uses Popovics (1973) curve, which describes the behaviour of both the confined and unconfined concrete, as shown in Fig. 5a. In the confined concrete model, confinement parameters due to transverse reinforcement proposed by Mander et al (1988a) are considered. Tensile stress-strain behaviour of concrete is also included in the numerical analysis, which is taken from the linear-elastic range of the test results. For the stress-strain behaviour of longitudinal reinforcement, the *Reinforcing steel material* model proposed by Kunnath et al (2009) was used to describe the nonlinear behaviour of the reinforced fibers as shown in Fig. 5c.

To simulate accurately the bond-slip effect of reinforcing bars, the uniaxial material model Bond_SP01, developed by Zhao and Sritharan (2007), is incorporated into the numerical model. The bond-slip behavior defined in Fig. 5 d was incorporated into the numerical model through a zero-length section element placed between the fiber-based column element and the rotational spring, as shown in Fig. 4. The zero-length section element is an independent fiber section with unit length and consists of concrete and reinforcing steel fibers represented by the bond-slip material model.

To simplify the nonlinear behavior, the rotational behavior of the column embedded connection was taken into account. The numerical representation of this rotation ultimately consists of a spring. Rotational springs are located at the column base and assigned as zero-length elements to consider rotational behavior, as shown in Fig. 4. In this study, elastic material in OpenSees, as shown in Fig. 5b, is used to define the stiffness of the embedded region. A simplified method for predicting the rotational stiffness of the spring is given in detail in the previous section.

Simulation of the numerical models is necessary to generate realistic results. In alignment with the above discussion, the fiber-based model established in OpenSees based on geometric and material properties was considered for prediction. The numerical analyses were conducted on precast columns in socket foundations selected from the study by Karadoğan et al (2013), and the material model and properties used are summarized in Table 2. In these analyses, Eq. 6 was employed to calculate the rotational stiffness at the socket–foundation connection. The rotational stiffness (β) values obtained using this equation were determined to be 1.047×10^5 kNm/rad for the S30_1416 column and 2.355×10^5 kNm/rad for the S40_20 column. For comparison, the rotational stiffness values were also directly

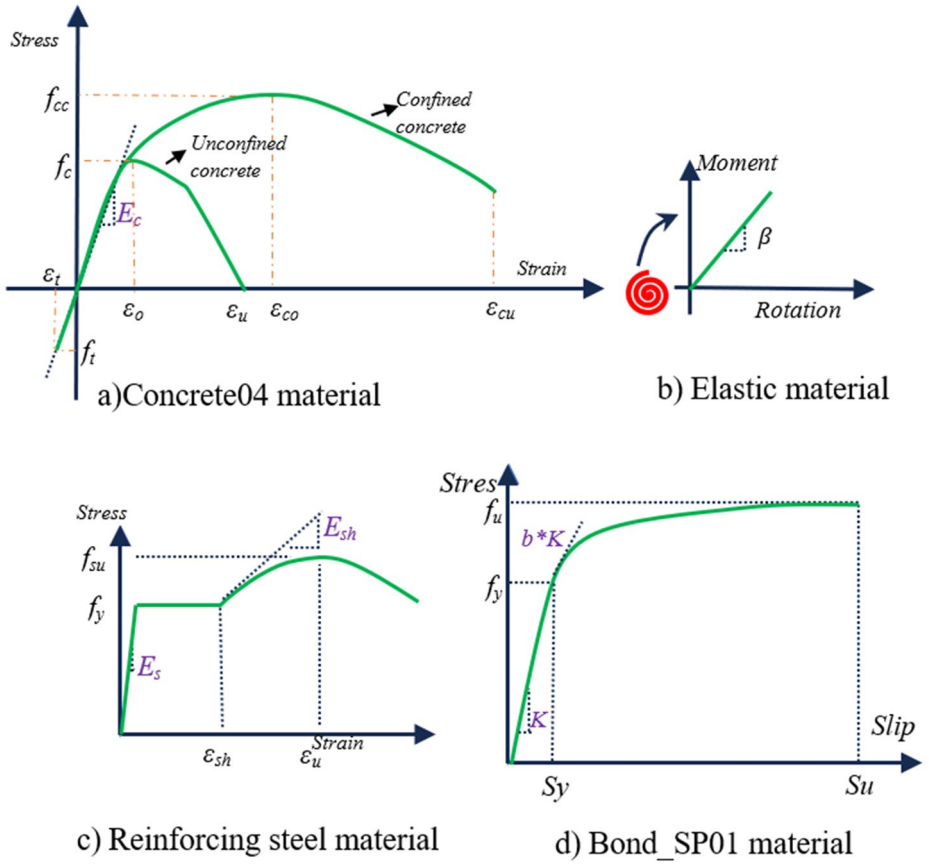

Fig. 5 Material models

obtained from the experimental results by considering the initial slope at the cracking point of the lateral force–displacement curves. These values were found to be 1.513×10^5 kNm/rad and 1.925×10^5 kNm/rad for the S30_1416 and S40_20 columns, respectively. The differences between the predicted and experimental results (with Eq. 6 to experimental ratios of 0.7 and 1.22) can be attributed to the error rates illustrated in Fig. 2.

The obtained results were compared with the experimental data in terms of the lateral force–displacement relationship. Figure 6 illustrates the comparison of hysteretic curves between the experimental and numerical results. The fiber-based model provides an accurate representation of the hysteretic response of precast columns and captures the cyclic behavior of experimental results during the loading and unloading steps.

Table 2 Material model parameters

Specimen	Material model	Parameters					
		f_y (Mpa)	f_{su} (MPa)	E_s (MPa)	E_{sh}(MPa)	ε_{sh}	ε_{ult}
S35_1416	Reinforcing Steel	479	598	200000	3000	0.008	0.08
S40_20		540	658	200000	3000	0.008	0.08
		f_y (MPa)	S_y (mm)	f_u (MPa)	S_u (mm)	b	R
S35_1416	Bond_SP01	479	0.39	598	13	0.5	0.8
S40_20		540	0.51	658	18	0.5	0.7
		E_c (MPa)	f_c (MPa)	f_t (MPa)	ε_t	ε_o	ε_u
S35_1416	Concrete 04 (Unconfined)	33838	45.8	5.0	0.00014	0.002	0.005
S40_20		34532	45.9	5.0	0.00014	0.002	0.005
		E_c (MPa)	f_{cc} (MPa)	f_t (MPa)	ε_t	ε_{co}	ε_{cu}
S35_1416	Concrete 04 (Confined)	33838	54.0	5.0	0.00014	0.004	0.015
S40_20		33874	53.3	5.0	0.00014	0.004	0.013

Note: f_y=yield strength of steel; f_{su}, f_u=ultimate strength of steel; E_s=Young's modulus of steel; E_{sh}=Tangent at initial strain hardening; ε_{sh}=strain corresponding to initial strain hardening; ε_{ult}=strain corresponding to peak stress; S_y=rebar slip at member interface under yield stress; S_u=rebar slip at the loaded end at the bar fracture strength; b= Initial hardening ratio in the monotonic slip vs. bar stress response; *R*= pinching factor for the cyclic slip vs. bar stress response; E_c=elastic modulus of concrete; f_c and f_{cc}=compressive strength of unconfined and confined concrete, respectively; f_t=tensile strength of concrete; ε_t=tensile strain of concrete; ε_o and ε_{co}=strain at maximum strength for unconfined and confined concrete, respectively; ε_u and ε_{cu}=ultimate strain for unconfined and confined concrete, respectively

4 Damage states

The nonlinear behavior and damage states of structures under seismic loads can be determined and classified through static or dynamic nonlinear analyses within the framework of performance-based design. Especially, establishing several performance levels and quantifying the associated deformations for each level, indicative of various damage states, is essential for evaluating and building seismic-resistant structures. When the seismic response of the structure exceeds specified limit values, damage conditions indicate that a particular performance level has been reached. In this study, material strains are used to determine damage level because they provide a critical measure of the severity of damage for primary structural elements. Priestley (2002) and Calvi et al (2007) indicated that displacements and material strains are significantly correlated in evaluating the damage potential of structures.

In determining the material's limit deformations that govern the damage states, critical concrete and reinforcement strain were considered. The four different damage states were defined individually as follows. The first limit state, DS1, is related to the cracking of cover concrete, characterized by the development of flexural cracks and linear elastic behavior. The second limit state, DS2, occurs at the point of yielding when the longitudinal reinforcement fiber of the column reaches its yield strain. Limit state DS3 is defined with the cover concrete begins to spall when the exterior fiber reaches the compression strain limit. Final one DS4, these performance limit states were considered when crushing of confined concrete and buckling of longitudinal reinforcement concentrated in the plastic hinge zone. This ultimate damage state can significantly affect the strength and stiffness, and bring the column specimen near collapse.

The drift ratios of the precast concrete columns were estimated for each performance level utilizing concrete and reinforcement material deformation limits. Yield strain was

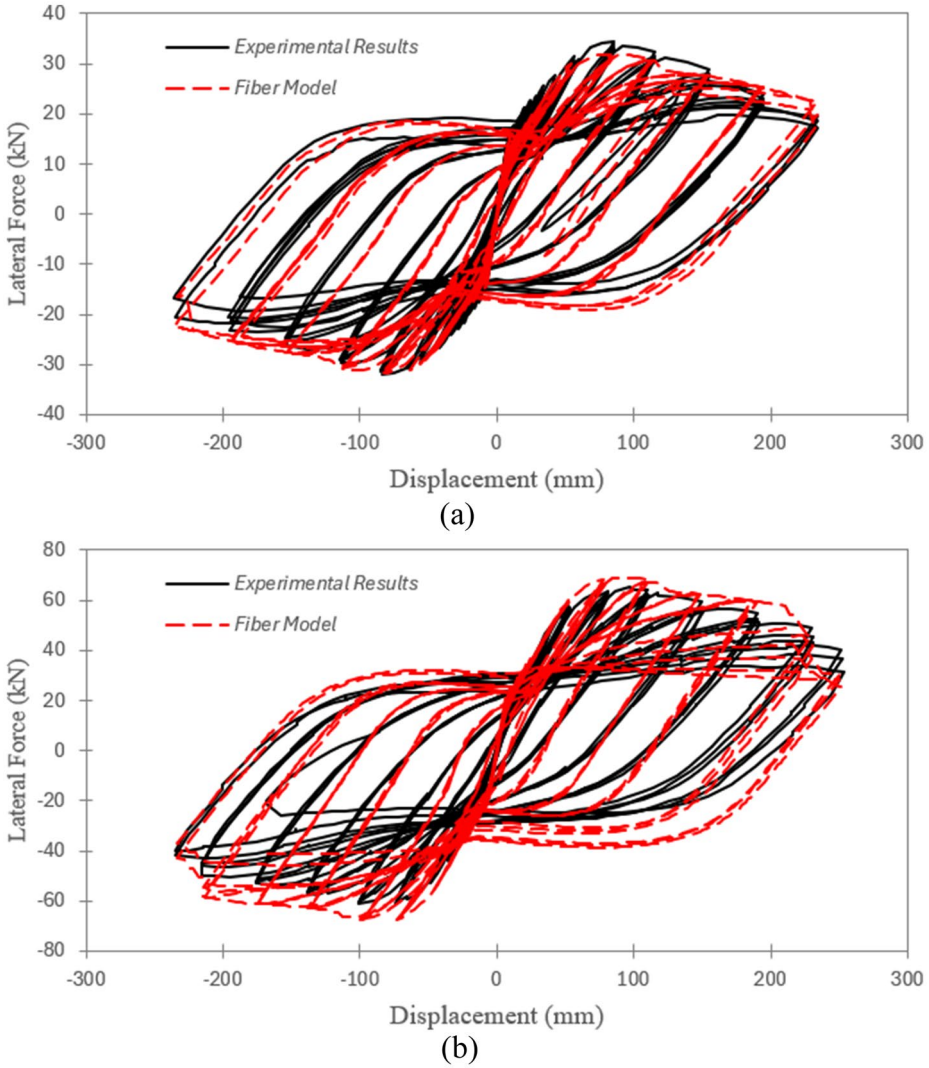

Fig. 6 Comparisons of fiber model and experimental results for (**a**) S35_1416 (Karadoğan et al 2013); (**b**) S40_20 (Karadoğan et al 2013)

determined based on the yield strength and the corresponding elastic modulus of steel. Spalling of cover concrete is another indicator of damage. According to (Crowley et al 2004), strain limits for concrete cover spalling can be taken as 0.004–0.005. In this study, the spalling strain of the cover concrete is assumed to be 0.005.

Several empirical models have been proposed in the literature to predict the strain corresponding to the buckling of longitudinal reinforcement, based on experimental results (Bae et al 2005, Feng et al. 2015; Bournas and Triantafillou 2011; Rodriguez et al 1999; Rodriguez and Iñiguez 2019; Urmson and Mander 2012). In addition, Jiang et al. (2010) focused specifically on flexure-controlled reinforced concrete columns and proposed an equation to

estimate the strain at the onset of reinforcement buckling. This equation, which was developed using observations of longitudinal reinforcement buckling from the PEER database (Berry et al. 2004), is presented in Eq. (7). In this equation, K_e represents the confinement effectiveness coefficient defined by Mander et al (1988a), and s/d_b denotes the ratio of transverse reinforcement spacing to the longitudinal bar diameter.

$$\varepsilon_{bb} = 0.0023 + 0.0572\, {K_e}^2 \left(\frac{s}{d_b}\right)^{-\frac{1}{4}} \tag{7}$$

Lastly, Crowley et al (2004) suggested that concrete strain limits of confined members may occur between 0.010 and 0.020. In this study, the crushing strain of core concrete was taken from a commonly used equation proposed by Paulay and Priestley (1992) and given in Eq. (8). The drift at the strain-based damage states is obtained by tracking the strain formation in the corresponding material strain (reinforcement and concrete) on the fiber-based modeling of the precast column.

$$\varepsilon_{cu} = 0.004 + \frac{1,4\rho_s f_{yh} \varepsilon_{sm}}{f_{cc}} \tag{8}$$

Where, ρ_s is the volumetric ratio of transverse steel, f_{yh} is the yield stress of transverse steel, ε_{sm} is the ultimate tensile strain of steel, and f_{cc} is confined concrete compressive strength. The four-performance limit states, which represent damage control, as well as their strain limit criterion, were defined for the precast columns in socket foundations as stated in Table 3.

4.1 Design parameters of precast columns

To provide a comprehensive database of precast concrete columns, various types of columns with different properties were generated for analysis. While deciding on the design parameters in this study, information obtained from past studies in Türkiye and Italy examining precast structure members was used (Senel and Kayhan 2010; Palanci 2010; Palanci and Senel 2013; Yeşilyurt et al 2021; Deyanova et al 2023; Arslan et al 2024). According to data obtained from single-story precast structures, Deyanova et al (2023) observed that precast columns have relatively large aspect ratios, mostly ranging between 10 and 20. In addition, Yeşilyurt et al (2021) reported the mean and standard deviation (SD) values of column dimensions and heights in their investigations on precast structures. Based on these values, when the aspect ratios were classified, it was observed that the mean aspect ratios of prefabricated columns were distributed between approximately 10 and 20, within the associated error bars (±2SD) (Fig. 7). Furthermore, investigations on column cross-

Table 3 Damage states definition

Degree state	Degree of limit state	Damage Description	Stain Limit	
Slight	DS1	Cracking of the cover concrete	Concrete	$\varepsilon_c = \varepsilon_{cr}$
Minor	DS2	Yielding of rebars	Steel	$\varepsilon_s = \varepsilon_{yield}$
Moderate	DS3	Spalling of the cover concrete	Concrete	$\varepsilon_c = 0.005$
Severe	DS4	Crushing of core concrete	Concrete	$\varepsilon_c = \varepsilon_{cu}$
		Buckling of longitudinal rebars	Steel	$\varepsilon_s = \varepsilon_{bb}$

section dimensions by Yeşilyurt et al (2021) and Senel and Kayhan (2010) indicated that the majority of precast columns have square sections, with sizes ranging from 35 × 35 cm to 60 × 60 cm. Considering these parameters, three representative square-section columns (35, 50, and 60 cm) were selected for the modeling study, with corresponding aspect ratios of 10, 14, and 18, respectively.

Some past building investigations indicate that axial load levels in single-story precast structures are not critical; the mean axial load ratio may be considered as 5% (Palanci and Senel 2013). Distribution of axial load ratio was determined to be between %7.5% and 12.5% (Deyanova et al 2023; Palanci 2010). When examined in terms of longitudinal reinforcement ratios, the columns showed a range of 1% to 3% (Yeşilyurt et al 2021; Palanci 2010; Palanci and Senel 2013). Observations about the embedment depth of the columns indicated that it was generally 1.5 to 2.0 times the depth of the column, which meets the provisions of the Turkish Standard for precast structures (Arslan et al 2024). Based on the observations and studies given above, significant parameters that created column section models, including axial load ratio, concrete strength, reinforcement yield strength, column aspect ratio, embedment depth-to-column depth ratio, longitudinal reinforcement, and transverse reinforcement ratio, are given in Table 4.

4.2 Pushover analysis

To investigate the influence of key design parameters, a total of 2916 square-section column models were developed by considering all possible combinations of the eight variables presented in Table 4, and each model was subjected to pushover analysis. The strain demands in the concrete and reinforcement at the fiber sections for each column were determined and compared with the strain limits corresponding to the different damage states listed in Table 3. Subsequently, the drift demands associated with each damage state (DS) were identified

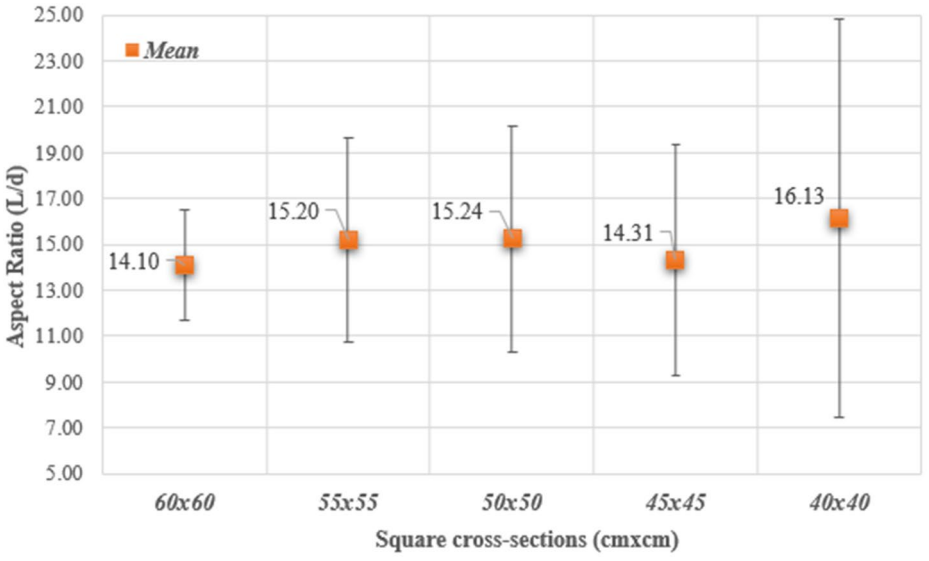

Fig. 7 Descriptive error bars illustrating mean aspect ratio and variability (±2SD) for different column cross-sections

Table 4 Precast column models corresponding to different parameters

Parameters	Symbol	Unit	1	2	3
Square column section depth	d	m	0.35	0.50	0.60
Axial Load Ratio	$N/(A_g f_c)$	-	0.05	0.1	0.15
Longitudinal reinforcement ratio	p	%	1.00	1.63	2.44
Transverse reinforcement ratio	p_w	%	0.35	0.78	1.22
Concrete strength	f_c	MPa	25	45	
Reinforcement Yield strength	f_y	MPa	420	500	
Column aspect ratio	*L/d*	-	10	14	18
Embedment depth to column depth ratio	*l/d*	-	1.0	1.5	2.0

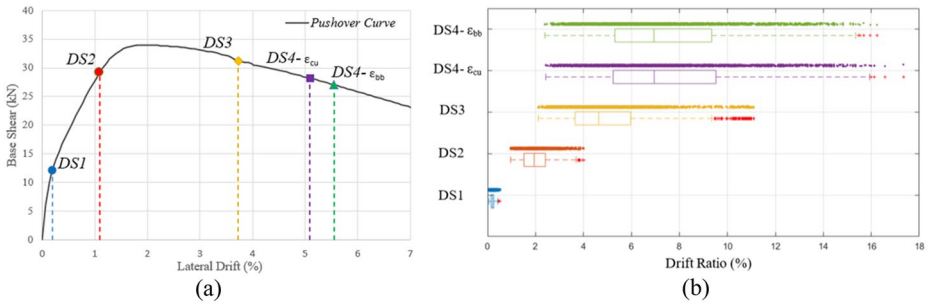

Fig. 8 (**a**) Pushover response for a selected representative column and (**b**) damage state results based on the drift ratio

from the pushover curve. As an illustrative example, the pushover curve and damage state limits for a selected representative column are presented in Fig. 8a. Based on the analysis results for all columns, the distribution of damage states in terms of drift demand is shown in Fig. 8b.

Figure 8 demonstrates data points and box plots to provide information about each damage state. The middle line of the box plot represents the median of the data points, while the left and right borders of the box display the values at which the 25th percentile of the data falls below and above, respectively. The figure also shows the lowest and highest data points, excluding outliers. Outliers beyond these limits are marked with red lines. Damage State DS1 occurs at low displacements, with drift ratios ranging between 0.06% and 0.53%. This damage state can be considered as slightly damaged or undamaged, as the expected structural response remains linear elastic. Therefore, the focus of the investigation was concentrated on the other damage states (DS2, DS3, and DS4), which have a greater influence on seismic behavior. Drift ratio for second damage state, DS2, can range from 0.96% to 3.7% and the drift ratio associated with DS3 can range from 2.11% to 9.35%. Excluding outliers, the drift ratio corresponding to the fourth and final damage state, DS4, ranges from 2.43% to 15.93% for core concrete crushing (ε_{cu}) and from 2.39% to 15.35% for buckling of the longitudinal reinforcement (ε_{bb}).

5 Empirical equations for estimation of drift limits

Deformations at performance limit states can be simplified and mathematically formulated for rapid assessment of precast columns in socket foundations. Thus, variation of the drift ratios associated with the yielding, spalling, crushing, and ultimate tensile strain limits was investigated statistically. The precast column data obtained from static pushover analysis were used to develop predictive expressions. The data were taken from previous studies, which were generated by statistically collecting geometric and mechanical information about precast structures. These data include 2916 analyses with combinations of different variables.

In this study, the Response Surface Methodology (RSM) was utilized to develop predictive equations for drift ratios, based on the principle of applying polynomial regression to the data in cases where a response is influenced by multiple independent variables (Bezerra et al 2008). RSM was preferred due to its ability to provide a more effective method for predicting the performance of data sets through polynomial regression, and it is reliable, practical, and easy to apply (Nooraziah and Tiagrajah 2014; Kalita et al 2019). In the regression analyses, the general polynomial form used to estimate the displacement capacities of precast columns is given in Eq. 9. The polynomial equation consists of linear and quadratic terms. In the given equation, x_i and x_j represent the independent variables of the mathematical model. α_i, α_{ii} ve α_{ij} correspond to the regression coefficients, α_0 is the constant term, and y is the predicted variable expression.

$$y = \alpha_0 + \sum \alpha_i x_i + \sum \alpha_{ii} x_i^2 + \sum \alpha_{ij} x_i x_j \tag{9}$$

The Analysis of Variance (ANOVA) was used to statistically examine the parameters of the polynomial regression model and to determine whether the effects of these parameters on the damage limit states were significant (Montgomery 2013). The analyses were conducted with a 95% confidence level, and the statistical significance of the parameters was evaluated based on whether their p-values were less than 0.05. As a result of the analyses, the parameters with p-values greater than 0.05, which do not have a significant contribution in each drift damage state, are shown with dashed lines, while the statistically significant parameters and their percentage contributions are presented in Fig. 9. However, although some parameters at the damage limits were statistically significant, their percentage contributions to the results might be low. In Fig. 9, the main factors that significantly affect the performance of

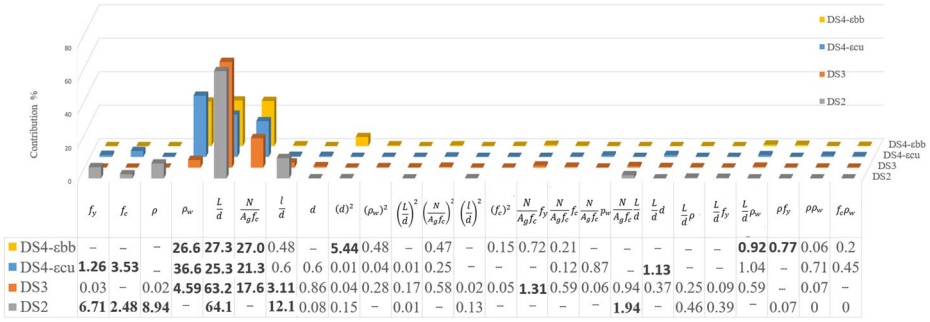

Fig. 9 Percentage contributions of various parameters in different damage states

precast columns and thus their drift ratios are highlighted in bold. It was also observed that linear terms had a more pronounced and significant effect on drift ratios than the quadratic terms.

As a result of the ANOVA analyses, regression analyses were performed by considering the statistically significant parameters with the highest percentage contributions. This approach is important for reducing the complexity of the equations and for evaluating the parameters that provide meaningful contributions. The proposed simplified equations for predicting the drift ratios corresponding to four damage states, rebar yielding, cover concrete spalling, core concrete crushing, and rebar buckling are presented in Eqs. (10–13). All regression and ANOVA analyses were conducted utilizing the Minitab v22 (2025) statistical software package.

$$\frac{\Delta_y}{L}(\%) = -1.182 + 0.004f_y - 0.009f_c + 0.296\rho + 0.129\frac{L}{d} - 0.496\frac{l}{d} + 0.138\left(\frac{N}{A_g f_c}\frac{L}{d}\right) \quad (10)$$

$$\frac{\Delta_{spal}}{L}(\%) = 1.382 + 0.039\left(\frac{N}{A_g f_c}f_y\right) + 1.016\rho_w + 0.374\frac{L}{d} - 33.355\frac{N}{A_g f_c} - 0.646\frac{l}{d} \quad (11)$$

$$\frac{\Delta_{cu}}{L}(\%) = -1.493 + 0.222\frac{L}{d}d - 0.057f_c - 33.327\frac{N}{A_g f_c} + 0.367\frac{L}{d} + 5.077\rho_w + 0.008f_y \quad (12)$$

$$\frac{\Delta_{bb}}{L}(\%) = 3.066 + 7.101d^2 + 0.243\left(\frac{L}{d}\rho_w\right) + 0.90\rho_w + 0.28\frac{L}{d} - 37.756\frac{N}{A_g f_c} - 0.0009\rho f_y \quad (13)$$

As can be seen from Fig. 9, the aspect ratios (L/d) of the columns have the greatest influence on the different damage states. Specifically, for DS2 and DS3, the contributions were over 63%, while for DS4-ε_{cu} and DS4-ε_{bb}, this rate dropped to approximately 25% due to the influence of other parameters. This indicates that the increase in the L/d ratio corresponds to a significant increase in the damage limits. Previous experimental and analytical studies have observed that the effect of the aspect ratio is a key parameter and has a significant influence on the obtained column drift ratio (Kowalsky 2000; Berry and Eberhard 2003, Sezen and Moehle 2004; Raza et al. 2018; Ying and Jin-Xin 2018). For example, Kowalsky (2000) stated that when the column aspect ratio exceeds 6, drifts significantly increase, and larger elastic flexibility and deformation effects occur on the columns.

It is also seen that the transverse reinforcement ratio (ρ_w) is among the other significant contributing parameters for DS3, DS4-ε_{cu}, and DS4-ε_{bb}. There is a positive correlation between the damage states and the increase in transverse reinforcement, and the increase leads to larger drift ratios in the damage states. Similarly, previous studies have also shown that transverse reinforcement ratios are an important variable controlling displacements caused by reinforcement buckling, and an increase in the transverse reinforcement ratio leads to higher drift ratios (Grira and Saatcioglu 1999; Berry and Eberhard 2005; Lehman et al 2004). In the ultimate concrete strain equation proposed by Paulay and Priestley (1992), the proportional relationship between ρ_w and ε_{cu} has led to an increase in drift ratios for the DS4-ε_{cu} damage state, contributing 36.6%.

Furthermore, the comprehensive parametric study conducted by Paultre and Légeron (2008) demonstrated that confinement effectiveness coefficient K_e systematically varies

with the section area ratio for different cross-section dimensions. Accordingly, the presence of the K_e term in the buckling strain equation and the contribution of section area to 5.47% of the variance for the DS4–ε_{bb} damage state, confirms that cross-section dimensions have an indirect but meaningful impact on the buckling performance. Similarly, Mander et al (1988b) reported that transverse reinforcement configuration strongly influences K_e. Considering the indirect influence of the transverse reinforcement ratio (ρ_w) on K_e, it can be concluded that ρ_w makes a substantial contribution to the variance associated with the DS4–ε_{bb} damage state. Moreover, the s/d_b ratio may also exert an indirect influence on the DS4–ε_{bb} variance through its interaction with both longitudinal and transverse reinforcement ratios. In this context, the notable contribution of approximately 27% (as shown in Fig. 9) attributed to ρ_w highlights the dominant role of transverse reinforcement ratio in governing the buckling behavior of precast concrete columns.

Regarding the axial load ratio ($N/A_g f_c$), it is observed to have a significant effect on the drift ratios for DS3, DS4-$\varepsilon_{cu,}$ and DS4-ε_{bb}. Together with the column aspect ratio (L/d), the axial load ratio is identified as one of the two most critical parameters affecting the spalling of cover concrete, contributing approximately 63.2% and 17.6%, respectively. This result was consistent with the empirical expression proposed by Berry and Eberhard (2003) for predicting the spalling of cover concrete. According to Ying and Jin-Xin (2018), the decreasing effect of the increase in the axial load ratio on the drift ratios and deformation capacity was associated with a decrease in the stiffness strength and a more dominant shear behavior with the pinching effect of hysterical loops. Additionally, for the DS4-ε_{bb} damage state, the axial load ratio ($N/A_g f'_c$) had a negative impact on the drift ratios, contributing 26.8% to the total variance. This indicates that an increase in the axial load ratio leads to earlier buckling of the reinforcement. Some studies have also shown that an increase in axial force accelerates buckling and reduces the deformation capacity of the column. (Ying and Jin-Xin 2018; Goodnight 2015; Berry and Eberhard 2005).

As for the embedment depth ratio (l/d) of precast columns, it was observed that changes in embedment depth between 1.0d-2.0d exhibited similar seismic performance for precast columns in socket foundations in the final damage state associated with DS4. However, while the effect on DS2 and DS3 was more significant than on DS4 damage state, the percentage contributions at 12.1% and 3.11%, respectively. In both damage states, the increase in the embedment depth and hence the stiffness of the socket connection led to a positive increase in drift ratios. Previous studies (Osanai et al 1996; Canha et al 2009; Xu et al 2021) have shown that with decreasing embedment depth, stiffness degradation in socket columns started earlier, and strains in longitudinal reinforcement at the column base were observed to be larger.

The correlation between the predicted and measured values using the proposed equations is comparatively presented in Fig. 10. The squares of the correlation coefficient (R^2) in the empirical equations presented as a function of different variables are also shown in the Fig. 10. The R^2 values range from 0.88 to 0.96, indicating that the points are not scattered and there is a good correlation between the predicted values and the numerical results

In order to better assess the accuracy of the proposed equations, a comparison was made between the parametric equations and various experimental results. In previous studies on socket-based precast column tests (Karadoğan et al 2013; Palermo et al 2007; Metelli et al 2011), yielding of reinforcement (DS2), spalling of cover concrete (DS3), and buckling of reinforcement (DS4-ε_{bb}) were reported. However, due to the more subjective approaches of

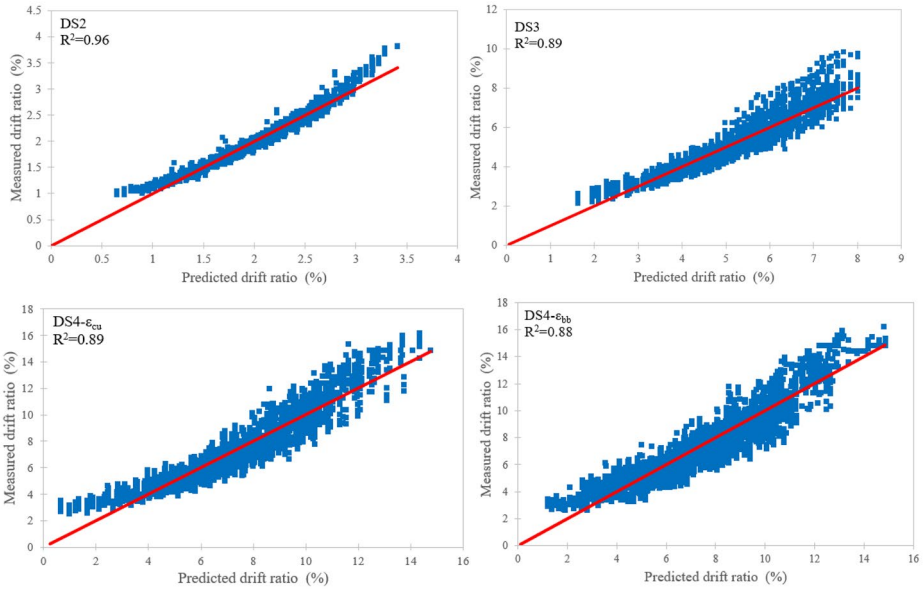

Fig. 10 Measured and predicted drift ratios for different damage states

the experimental data related to the crushing of core concrete (DS4-ε_{cu}), there has not been a clear experimental report corresponding to the drift ratio for this damage state. Table 5 presents the properties of the experimentally tested square-section precast column specimens along with the corresponding drift ratios for each damage state and compares these experimental results with the predictions of the proposed equations. Figure 11 shows the error rates between the predicted values obtained from the equations and the experimental data. When evaluating the damage states, the error rates for DS3 and DS4-ε_{bb} were observed to range between 1.42% and 35.89%. In the case of the DS2 damage state, which corresponds to the yielding of reinforcement, the error rates ranged from 0.02% to 33.7%. Overall, the average error rates were calculated as 11% for DS2, 11% for DS3, and 12% for DS4-ε_{bb}. These results show that the drift ratios predicted by the proposed equations are in good agreement with the experimental data and can be predicted with sufficient accuracy.

6 Fragility curves for precast columns

As discussed in the previous sections, determining deformation limits helps engineers identify areas that may have experienced structural damage. In the analyses, material strain limits were used as a basis to determine the drift ratio corresponding to the damage levels in the plastic hinge region of the precast columns in socket foundations. It will be important to identify appropriate probabilistic distributions for each damage level calculated based on strain limits and to analyze them statistically. For this purpose, fragility curves based on drift demands can be developed to estimate the likelihood of reaching or exceeding these damage levels of precast columns. In this regard, drift-based fragility curves may be useful for structural performance evaluation of the socket column under seismic loading conditions.

Table 5 Comparison between drift ratios obtained from experimental and predicted results

Sample Number	Experimental test	Test ID	Parameters								DS2		DS3		DS4-ε_{bb}	
			f_y (MPa)	f_c (MPa)	ρ (%)	ρ_w (%)	$\frac{L}{d}$	$\frac{N}{A_c f_c}$	d (m)	l /d	Exp. (%)	Pred. (%)	Exp. (%)	Pred. (%)	Exp. (%)	Pred. (%)
1	Karadoğan et al (2013)	S30_14	479	45.9	1.37	0.58	12.57	0.03	0.30	2.33	1.46	1.24	4.51	4.70	7.00	7.77
2		S30_16	502	44.2	1.79	0.58	12.57	0.05	0.30	2.33	1.46	1.50	4.14	4.54	7.43	7.03
3		S30_18	452	45.8	2.26	0.58	12.57	0.05	0.30	2.33	1.46	1.43	4.03	4.37	7.43	6.72
4		S35_18	452	45.8	1.66	0.49	10.77	0.05	0.35	2.00	1.03	1.17	3.90	3.83	6.63	6.14
5		S35_20	540	45.8	2.05	0.49	10.77	0.05	0.35	2.00	1.46	1.64	3.93	4.00	6.63	5.84
6		S40_16	502	45.9	1.01	0.42	9.43	0.05	0.40	1.75	1.41	1.12	2.92	3.52	6.15	5.87
7		S40_20	540	45.9	1.57	0.42	9.43	0.05	0.40	1.75	1.41	1.44	3.98	3.59	6.66	5.58
8		S40_2020	540	45.9	2.36	0.56	9.43	0.05	0.40	1.75	1.62	1.67	2.76	3.73	6.55	5.66
9		S35_1416	479	45.8	1.16	0.49	10.77	0.05	0.35	2.00	1.14	1.13	4.11	3.88	6.21	6.30
10	Palermo et al (2007)	Prototype 1	555	46	1.01	0.60	12.5	0.02	0.40	2.5	2.00	1.33	--		6.50	8.83
12	Metelli et al (2011)	PF	555	51	1.50	0.57	7.11	0.06	0.45	1.56	1.30	1.13	--		--	

Previous studies in engineering research have developed drift-based fragility functions for the performance evaluation of reinforced concrete elements. Aslani (2005) developed drift-based fragility curves for specific damage states related to non-ductile reinforced concrete columns and slab-column connections based on an experimental database. Zhu (2005) developed fragility curves for key parameters, including the aspect ratio, based on a 20% reduction in the horizontal load capacity of reinforced concrete columns. It was determined that the aspect ratio caused wider dispersion in the fragility curves, and changes in column height created significant differences in the collapse probability for the same drift demand. Ruiz-García and Ramos-Cruz (2024) presented drift-based fragility curves for reinforced concrete columns with low ductility levels, obtained from experimental data. In the study, the impact of column aspect ratio and axial load ratio on the fragility curves was investigated. In the evaluation of damage states, it was determined that columns with an aspect ratio greater than 2 had lower exceedance probabilities compared to those with a lower aspect ratio.

Using the drift values corresponding to each damage state calculated for precast socket columns, the probabilities of exceeding these damage states were determined by the cumulative distribution function (CDF), and drift-based fragility curves were generated. To evaluate damage probabilities based on drift values, theoretical fragility curves can be derived using Eq. 14 under the assumption of a lognormal distribution. In this equation, β and $\mu_{\ln(x)}$ are the standard deviation and the mean of the lognormal probability distribution corresponding to the drift-based damage states, respectively. ϕ denotes the standard normal cumulative distribution.

$$F\left(DS|\delta = x\right) = \phi\left(\frac{\ln\left(x\right) - \mu_{\ln(x)}}{\beta}\right) \tag{14}$$

Empirical cumulative distribution function of damage state was also plotted and calculated based on drift values. Sample data drifts were subsequently arranged in ascending order, associated probability was calculated with $(i-0.5)/(n)$, where i indicates the position of each the drift ratio (δ) and n is total number of specimen at given damage states. This approach illustrates the empirical cumulative distribution of drift ratio for different damage states.

Kolmogorov-Smirnov (K-S) goodness-of-fit test with 5% significance level was used to determine whether the lognormal distribution is appropriate to represent the empirical distribution (Benjamin and Cornell 2014). According to this hypothesis, if data points fall within lower and upper confidence bounds, the computed distributions are considered acceptable for the significance levels. Additionally, if the p-values obtained from the K-S test are greater than the 5% significance level, it indicates that the null hypothesis (H_0) is not rejected, and the distribution is appropriate for the data. The analysis showed that the lognormal distribution adequately represents the empirical distribution at the DS4 damage states.

In other damage states, it was observed that other probability distribution types were more suitable than the lognormal distribution for better representation. The 3-Parameter Weibull distribution aligns well with the data for DS2 and DS3 damage states. In addition to the scale and shape parameters of the two-parameter Weibull distribution, this distribution includes a location parameter that allows the distribution to be shifted along the horizontal

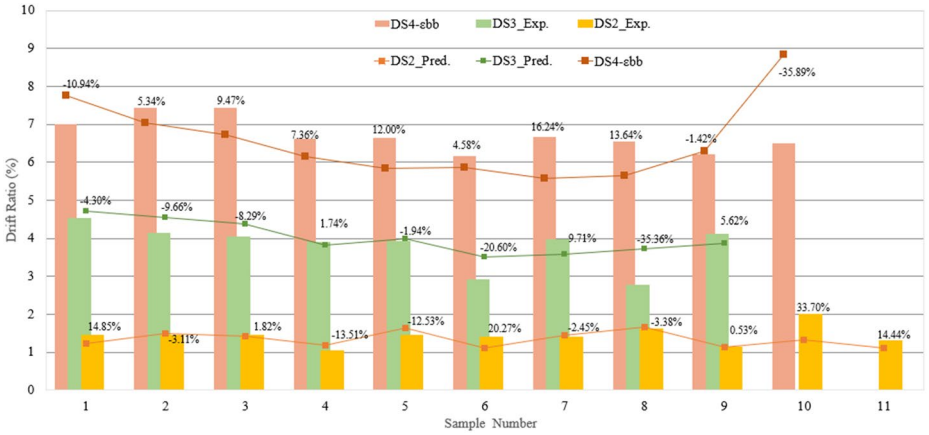

Fig. 11 Comparison of experimental and predicted results

axis, and the cumulative distribution function can be defined using all three parameters. It was observed that, above the location parameter, the distribution provides a good fit to both the probability and scatter of the observed damage data.

Figure 12 shows the graphical representation of the fragility curves and applied K-S tests at the 5% significance level. It can be observed that data points lie within the confidence bounds. Therefore, probability distributions are appropriate to describe the empirical distribution. As a result of all the K-S tests, fragility curves for DS2, DS3, and DS4 damage states were obtained and found to be suitable. Table 6 shows the statistical parameters of fragility curves obtained for the different damage states.

6.1 Influence of aspect ratio and embedment depth

The columns in precast structures, unlike traditional residential buildings, have much larger aspect ratios and often greater than 10, indicating that flexural behavior is more dominant in these columns. Although drift-based fragility curves have been developed for low aspect ratios ($L/d < 6$) in the literature (Aslani 2005; Zhu 2005; Ruiz-García and Ramos-Cruz 2024), considering the behavior of precast columns with high aspect ratios, it would be meaningful and effective to examine fragility curves for different L/d ratios. Also, as mentioned before, the aspect ratio has been highlighted as an important parameter controlling the drift ratios. As a second parameter, examining the effect of changes in the embedment depth ratio (l/d) on the exceedance probabilities of the damage states through fragility curves could be significant for evaluating the performance of precast socket columns and better understanding their behavior.

The relationship between drift ratio and damage states (DS2, DS3, DS4) along with the fragility curves of precast socket columns with different (L/d) and (l/d) ratios is presented in Fig. 13. The fragility functions and curves were developed following a procedure similar to that described in the previous section. Each graph representing a damage state shows the 5% confidence interval obtained using the Kolmogorov-Smirnov goodness-of-fit test, with these bounds indicated by dashed lines. All data points lie within these bounds, leading to the conclusion that the lognormal distribution provides a good fit and is an appropriate

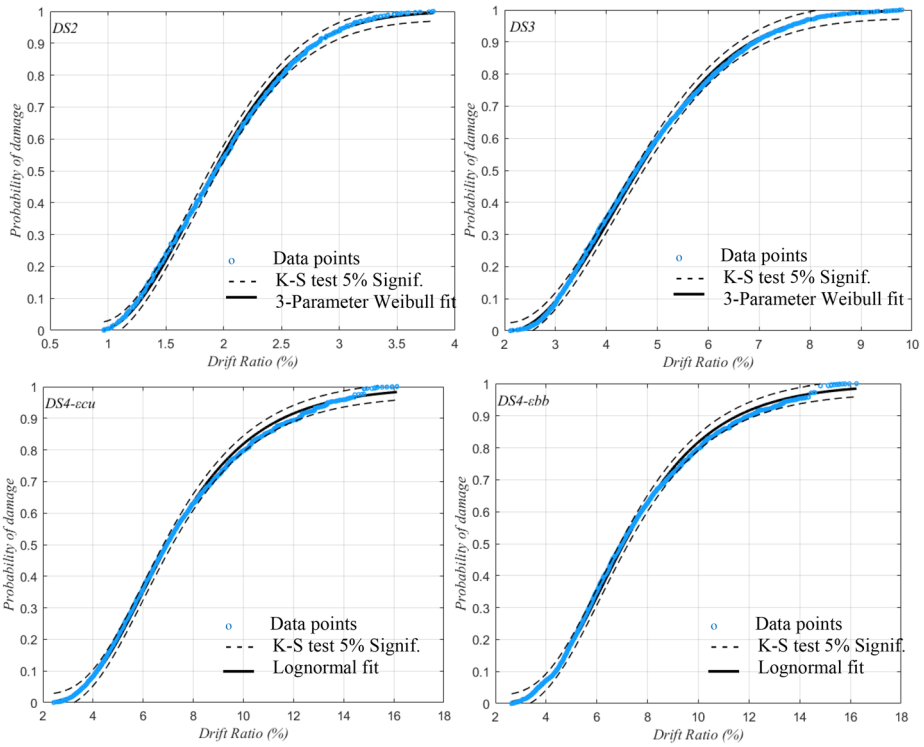

Fig. 12 Fragility curves for precast socket columns considering various damage states

Table 6 Statistical distribution parameters of different damage states

Damage State	Distribution	Location	Scale	Shape	Threshold	P value
DS2	3-Parameter Weibull	-	1.882	1.195	0.9319	0.052
DS3	3-Parameter Weibull	-	1.904	3.072	2.093	0.061
DS4-ε_{cu}	Lognormal	1.943	0.394	-	-	0.051
DS4-ε_{bb}	Lognormal	1.956	0.382	-	-	0.052

distribution type. The p-values corresponding to the statistical results after the K-S test are provided in Table 7.

According to the fragility analysis results, variations in the aspect ratio (L/d) led to significant differences in drift capacities in all damage states. In general, the fragility curves show that at the same damage level, as the aspect ratio increases from lower to higher values, the probability of reaching or exceeding a damage state occurs at larger drift ratios. For example, in the DS2 damage state and at the same embedment depth (l/d = 1.0), the drift ratio corresponding to a 50% exceedance probability is 2.89% for columns with a high aspect ratio (L/d = 18), while it drops to 1.59% when the aspect ratio decreases to L/d = 10. Similarly, in other damage states, columns show more fragility as the L/d ratio decreases.

Evaluating the fragility curves in terms of the embedment depth ratio, the higher percentage contributions observed in the DS2 and DS3 damage states resulted in a more pro-

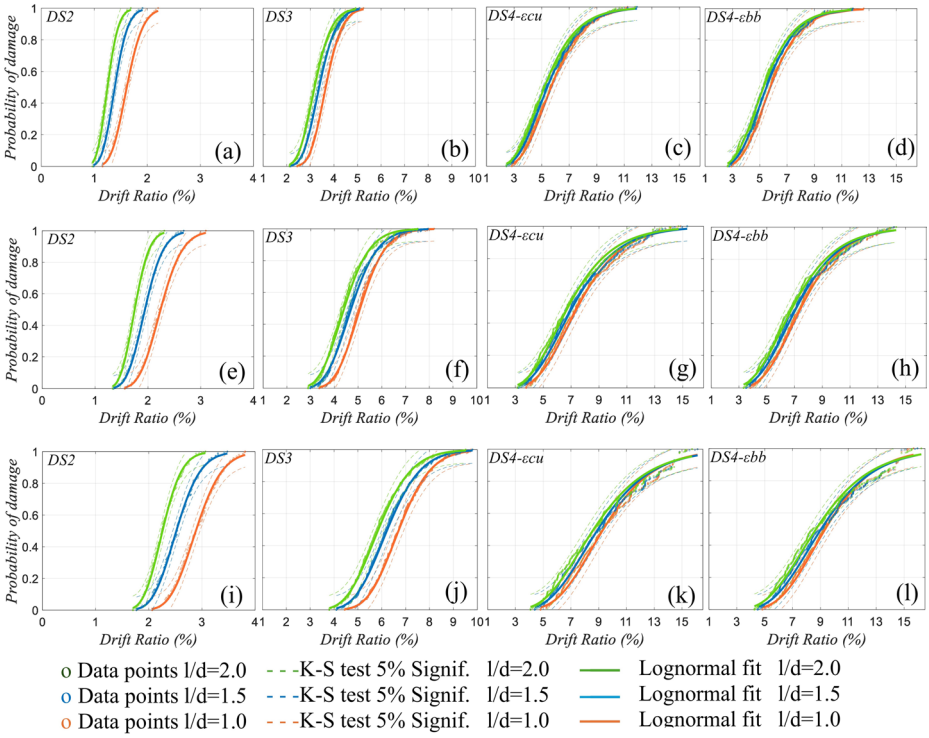

Fig. 13 Influence of aspect ratio (L/d) and embedment depth ratio (l/d) on drift-based fragility curves for precast socket column according to different damage states: (a-b-c-d) L/d = 10, (e-f-g-h) L/d = 14.0 and (i-j-k-l) L/d = 18.0

Table 7 p-values of K-S test for different aspect ratios and embedment depth ratios

Damage States	L/d = 10			L/d = 14			L/d = 18		
	l/d 1.0	l/d 1.5	l/d 2.0	l/d 1.0	l/d 1.5	l/d 2.0	l/d 1.0	l/d 1.5	l/d 2.0
DS2	0.206	0.328	0.262	0.449	0.608	0.590	0.312	0.377	0.546
DS3	0.677	0.698	0.551	0.430	0.302	0.240	0.971	0.798	0.758
DS4-ε_{cu}	0.789	0.820	0.768	0.489	0.625	0.553	0.141	0.054	0.150
DS4-ε_{bb}	0.525	0.481	0.435	0.567	0.536	0.431	0.173	0.160	0.139

nounced change in the fragility curves. The Fig. 13 shows that an increase in the embedment depth of the precast column caused a decrease in drift ratios. However, as the aspect ratio (L/d) decreases from 18 to 10, the variation in drift ratios at different embedment depths diminishes. This behavior is due to the fact that the theoretical column stiffness is inversely proportional to the cube of the column length. The increase in column height reduces the stiffness at the socket column-to-foundation connection, which leads to an increase in the drift ratios. Thus, at larger L/d ratios, a deeper embedment depth is required to meet the higher stiffness demand. For this reason, the fragility curves for different embedment ratios (l/d) exhibit less dispersion for columns with lower aspect ratios.

7 Conclusions

In this study, drift ratios were employed to define different damage states of square section precast columns in socket foundations, and simplified expressions were formulated to predict these damage states. Additionally, a theoretical equation was developed to estimate the stiffness of the socket connection by considering the moment-rotation relationship. The stiffness equation was integrated into the nonlinear behavior model, allowing the effect of the socket-foundation connection to be considered in the damage states. A database was created based on information obtained from the studies on precast structures in the literature, and column models incorporating various design parameters were generated. The nonlinear behavior of these columns was simulated using a fiber-based finite element model. The obtained results were subjected to statistical analyses to evaluate the effects of different parameters on the damage states and the developed expressions. The main conclusions from the analysis are as follows:

- When assessing the influence of various design parameters on damage states, the column aspect ratio (L/d) was found to significantly affect drift demands. Fragility curves also indicate that the reduction in drift ratios corresponding to different damage states becomes more pronounced.
- Changes in the embedment depth of the socket column influenced the damage states associated with longitudinal reinforcement yielding (DS2) and cover concrete spalling (DS3), while the ultimate drift capacity corresponding to DS4 showed negligible variation.
- The fragility curves also show that increasing the column length decreases the rotational stiffness of the socket-foundation connection, leading to higher drift ratios. As a result, larger embedment depths (l) are required for socket columns with high L/d ratios, especially for the DS2 and DS3 damage states.
- Comparisons with experimental results for the estimation of drift ratios corresponding to the damage states show that the column capacities are predicted with reasonable accuracy. The proposed equations can be used for the approximate estimation of damage states during the initial design phase of socket columns.
- The drift ratio equations formulated in this work are applicable only to flexure dominated square-section precast columns, and further investigation is needed to extend these models to rectangular-section columns. Additionally, the applicability of the proposed equations is limited to the parameter ranges employed in this study.
- In traditional designs and analyses, the rotational flexibility of socket–foundation connections is often neglected, and precast columns are assumed to be rigidly connected to the foundations. The simplified equation developed to predict the rotational stiffness of the socket–foundation connection can be used to account for connection flexibility in the design of columns and foundation. However, the behavior of the foundation–soil interface could be further investigated to assess its potential influence on column lateral deformations and damage states.

Author contributions Halil Dinçer: Conceptualization, Methodology, Writing, Original draft preparation, Formal analysis, Investigation, Resources, Sadık Can Girgin: Conceptualization, Methodology, Writing - review and editing

Funding The authors declare that no funds, grants, or other support were received during the preparation of this manuscript.

Data availability The datasets generated during and/or analysed during the current study are available from the corresponding author on reasonable request

Declarations

Competing interests The authors have no relevant financial or non-financial interests to disclose

References

Adalier K, Aydingun O (2001) Structural engineering aspects of the June 27, 1998 Adana-Ceyhan (Turkey) earthquake. Eng Struct 23:343–355

Arslan MH, Dere Y, Ecemiş AS, Doğan G, Özturk M, Korkmaz SZ (2024) Code-based damage assessment of existing precast industrial buildings following the February 6th, 2023 Kahramanmaraş earthquakes (Pazarcık Mw 7.7 and Elbistan Mw7. 6). J Build Eng 86:108811

Aslani H (2005) Probabilistic earthquake loss estimation and loss disaggregation in buildings. Stanford University

Aydemir C, Aydemir ME, Arslan G (2023) Drift capacity and allowable axial load level of RC columns. InStruct 48:1072–1081

Bae S, Mieses AM, Bayrak O (2005) Inelastic buckling of reinforcing bars. J Struct Eng 131(2):314–321

Barnwell NV (2015) Experimental testing of shallow embedded connections between steel columns and concrete footings. Brigham Young University, Utah, United States

Benjamin JR, Cornell CA (2014) Probability, statistics, and decision for civil engineers. Courier Corporation, New York

Berry MP, Eberhard MO (2003) Performance models for flexural damage in reinforced concrete columns. Pacific Earthquake Engineering Research Center

Berry MP, Eberhard MO (2005) Practical performance model for bar buckling. J Struct Eng 131:1060–1070. https://doi.org/10.1061/(ASCE)0733-9445(2005)131:7(1060)

BerryM, Parrish M, Eberhard M (2004) PEER Structural performance database user's manual. Pacific Earthquake Engineering Research Center Report. http://nisee.berkeley.edu/spd

Berry MP, Eberhard MO (2006) Performance modeling strategies for modern reinforced concrete bridge columns

Bezerra MA, Santelli RE, Oliveira EP, Villar LS, Escaleira LA (2008) Response surface methodology (RSM) as a tool for optimization in analytical chemistry 76:965–977

Bournas DA, Triantafillou TC (2011) Bar buckling in RC columns confined with composite materials. J Compos Constr 15(3):393–403

Calvi GM, Priestley MJ, Kowalsky MJ (2007) Displacement-based seismic design of structures. In New Zealand conference on earthquake engineering, IUSS Press

Canha RMF, de Borja Jaguaribe Jr K, de Cresce El ALH, El Debs MK (2009) Analysis of the behavior of transverse walls of socket base connections. Eng Struct 31(3):788–798. https://doi.org/10.1016/j.engstruct.2008.11.008

Canha RMF, Ebeling EB, de Cresce El Debs ALH, El Debs MK (2009) Analysing the base of precast column in socket foundations with smooth interfaces. Mater Struct 42:725–737. https://doi.org/10.1617/s11527-008-9416-4

Cheng Z, Liu D, Li S, Wang J, Zhang J (2021) Performance characterization and design recommendations of socket connections for precast columns. Eng Struct 242:112537

Cogurcu MT, Uzun M (2022) Experimental investigation of a new precast column-foundation connection under cyclic loading. J Build Eng 50:104245

Crowley H, Pinho R, Bommer J (2004) A probabilistic displacement-based vulnerability assessment procedure for earthquake loss estimation. Bull Earthq Eng 2:173–219. https://doi.org/10.1007/s10518-004-2290-8

Deyanova M, Bellotti D, Nascimbene R, Pampanin S (2023) Performance-based assessment of slender reinforced concrete columns typical of precast industrial buildings. Bull Earthq Eng 21433–21471

Dhakal RP, Maekawa K (2002) Reinforcement stability and fracture of cover concrete in reinforced concrete members. J Struct Eng 128:1253–1262

Ebeling EB (2006) Analysis of precast columns base in the connection with socket foundation. São Carlos. 103p (Doctoral dissertation, MSc Thesis. School of Engineering of São Carlos, University of São Paulo)
Ertaş O (2005) Ductile beam-column connections in precast concrete moment resisting frames. PhD thesis Boğaziçi University, İstanbul, Türkiye
Fardis MN, Biskinis DE (2003) Deformation capacity of RC members, as controlled by flexure or shear. In Otani symposium, pp 511530
Feng Y, Kowalsky MJ, Nau JM (2015) Effect of seismic load history on deformation limit states for longitudinal bar buckling in RC circular columns. J Struct Eng 141(8):04014187
Fischinger M, Kramar M, Isaković T (2008) Cyclic response of slender RC columns typical of precast industrial buildings. Bull Earthq Eng 6:519–534. https://doi.org/10.1007/s10518-008-9064-7
Goodnight JC (2015) The effects of load history and design variables on performance limit states of circular bridge columns. North Carolina State University
Grira M, Saatcioglu M (1999) Reinforced concrete columns confined with steel or FRP grids. In Proceedings of the 8th Canadian Conference on Earthquake Engineering, pp 445–450
Han Q, Su S, Zhang G, Xu K, Wang L, Du X (2023) Stiffness evaluation of UHPC-filled socket column-foundation joints: numerical investigation and analytical model. Soil Dyn Earthquake Eng 172:108040
Haselton CB, Goulet CA, Mitrani-Reiser J, Beck JL, Deierlein GG, Porter KA, Stewart JP, Taciroglu E (2008) An assessment to benchmark the seismic performance of a code-conforming reinforced-concrete moment-frame building, PEER report 2007/12, Pacific earthquake engineering Research center. University of California, Berkeley, California
Hetényi M (1946) Beams on elastic foundation: theory with applications in the fields of civil and mechanical engineering. University of Michigan Press
Jiang H, Lu X, Kubo T (2010) Damage displacement estimation of flexure-dominant RC columns. Adv Struct Eng 13(2):357–368
Kalita K, Dey P, Haldar S (2019) Search for accurate RSM metamodels for structural engineering. J Reinf Plast Compos 38:995–1013
Karadoğan H, Yüce SZ, Yüksel E, Bal I, Hasel F (2013) Single story precast structures in seismic Zones-I. In 4th ECCOMAS thematic conference on computational methods in structural dynamics and earthquake engineering, COMPDYN 2013, Kos Island, Greece
Kashani MM, Lowes LN, Crewe AJ, Alexander NA (2016) Nonlinear fibre element modelling of RC bridge piers considering inelastic buckling of reinforcement. Eng Struct 116:163–177
Kowalsky MJ (2000) Deformation limit states for circular reinforced concrete bridge columns. J Struct Eng 126:869–878
Kunnath SK, Heo Y, Mohle JF (2009) Nonlinear uniaxial material model for reinforcing steel bars. J Struct Eng 135:335–343
Lehman D, Moehle J, Mahin S, Calderone A, Henry L (2004) Experimental evaluation of the seismic performance of reinforced concrete bridge columns. J Struct Eng 130:869–879
Mander JB, Priestley MJ, Park R (1988a) Theoretical stress-strain model for confined concrete. J Struct Eng 114:1804–1826
Mander JB, Priestley MJ, Park R (1988b) Observed stress-strain behavior of confined concrete. J Struct Eng 114(8):1827–1849
Metelli G, Beschi C, Riva P (2011) Cyclic behaviour of a column to foundation joint for concrete precast structures. Eur J Environ Civ Eng 15:1297–1318
Minitab LLC (2025) *Minitab statistical software* (version 22.4) [computer software]
Montgomery DC (2013) Design and analysis of experiments. Wiley, New York
Negro P, Mola E, Ferrara L, Zhao B, Magonette G, Molina J (2006) Seismic behaviour of precast structure with respect to EC8. Report of Sept. 2006 on precast prototype, project-contract G6RD-CT-2002-00857
Nooraziah A, Tiagrajah VJ (2014) A study on regression model using response surface methodology. Appl Mech Mater 666:235–239
Osanai Y, Watanabe F, Okamoto S (1996) Stress transfer mechanism of socket base connections with pre cast concrete columns. Struct J 93:266–276
Özden Ş, Atalay HM, Akpınar E, Doyranlı B, İmren Ö (2012) Betonarme prefabrik yapıların 23 Ekim 2011 Van depreminde gözlenen performansı (the observed performance of reinforced concrete precast structures during the October 23, 2011 Van earthquake). Beton Prefabrikasyon Dergisi 103:11–19 (in Turkish)
Palanci M (2010) Mevcut prefabrik sanayi yapılarının deprem performansının bina envanterlerine dayalı tahmini (Estimation of the seismic performance of existing precast industrial buildings based on building inventories). Master's thesis, Pamukkale Üniversitesi Fen Bilimleri Enstitüsü, Denizli, Türkiye (in Turkish)
Palanci M, Senel SM (2013) Rapid seismic performance assessment method for one-story hinged precast buildings. Struct Eng Mech 48:257–274

Palermo A, Carabellese A, Toniolo G (2007) Numerical validation of pseudo-dynamic and quasi-static cyclic tests on full-scale precast industrial building prototypes. In Proceedings of the 8th Pacific Conference on Earthquake Engineering, pp 5–7
Panagiotakos TB, Fardis MN (2001) Deformations of reinforced concrete members at yielding and ultimate. Struct J 98:135–148
Paulay T, Priestley MN (1992) Seismic design of reinforced concrete and masonry buildings. Wiley, New York
Paultre P, Légeron F (2008) Confinement reinforcement design for reinforced concrete columns. J Struct Eng 134(5):738–749
Petracca M, Candeloro F, Camata G (2017) STKO user manual. ASDEA Software Technology, Pescara, Italy
Polat G (2010) Precast concrete systems in developing vs. industrialized countries. J Civ Eng Manag 16:85–94
Popovics S (1973) A numerical approach to the complete stress-strain curve of concrete. Cem Concr Res 3:583–599
Priestley MN (2002) Direct displacement-based design of precast/prestressed concrete buildings. Pci J 47:66–79
Pul S, Husem M, Arslan ME, Hamzaçebi S (2014) An experimental study on different socket base connections under cyclic loading. Comput Concr 13:377–387
Raza S, Tsang HH, Wilson JL (2018) Unified models for post-peak failure drifts of normal- and high-strength RC columns. Mag Concr Res 70:1081–1101
Richards PW, Barnwell NV, Tryon JE, Sadler AL (2018) Flexural strength and stiffness of block-out connections for steel columns. Eng Struct 173:404–415
Rodriguez ME, Botero JC, Villa J (1999 1999) Cyclic stress-strain behavior of reinforcing steel including effect of buckling. J Struct Eng 125(6):605–612
Rodriguez ME, Iñiguez M (2019) Drift capacity at onset of bar buckling in RC members subjected to earthquakes. In: Concr struct earthq E. Springer Singapore, Singapore, pp 185–200
Ruiz-García J, Ramos-Cruz JM (2024) Drift-based fragility assessment of nonductile reinforced concrete columns failing in shear under cyclic loading. Eng Struct 302:117378
Saatcioglu M, Mitchell D, Tinawi R, Gardner NJ, Gillies AG, Ghobarah A, Anderson DL, Lau D (2001) The August 17, 1999, Kocaeli (Turkey) earthquake damage to structures. Can J Civ Eng 28:715–737
Senel SM, Kayhan AH (2010) Fragility based damage assesment in existing precast industrial buildings: a case study for Turkey. Struct Eng Mech 34:39–60
Sezen H, Moehle JP (2004) Shear strength model for lightly reinforced concrete columns. J Struct Eng 130(11):1692–703
Shrestha S, Pujol S (2023) Drift capacity of reinforced concrete columns. ACI Struct J 120:215–224
Tryon JE (2016) Simple models for estimating the rotational stiffness of steel column-to-footing connections. Brigham Young University, Utah, United States
Urmson CR, Mander JB (2012) Local buckling analysis of longitudinal reinforcing bars. J Struct Eng 138(1):62–71
Xu Y, Zeng Z, Wang Z, Ge J (2021) Experimental studies of embedment length of precast bridge pier with socket connection to pile cap. Eng Struct 233:111906. https://doi.org/10.1016/j.engstruct.2021.111906
Yeşilyurt A, Zulfikar AC, Tuzun C (2021) Seismic vulnerability assessment of precast RC industrial buildings in Turkey. Soil Dyn Earthquake Eng 141:106539
Ying M, Jin-Xin G (2018) Seismic failure modes and deformation capacity of reinforced concrete columns under cyclic loads. Period Polytech Civ Eng 62(1):80–91. https://doi.org/10.3311/PPci.9893
Yüce SZ (2010) Basitleştirilebilen betonarme sistemlerin deprem hesabı için yerdeğiştirmeleri esas alan bir yöntem. PhD Thesis Istanbul technical University, İstanbul, Türkiye
Zhang G, Han Q, Xu K, Du X, He W (2021) Experimental investigation of seismic behavior of UHPC-filled socket precast bridge column-foundation connection with shear keys. Eng Struct 228:111527
Zhao J, Sritharan S (2007) Modeling of strain penetration effects in fiber-based analysis of reinforced concrete structures. ACI Struct J 104:133–141
Zhu L (2005) Probabilistic drift capacity models for reinforced concrete columns. (Doctoral dissertation, University of British Columbia)

Publisher's Note Springer Nature remains neutral with regard to jurisdictional claims in published maps and institutional affiliations.

Springer Nature or its licensor (e.g. a society or other partner) holds exclusive rights to this article under a publishing agreement with the author(s) or other rightsholder(s); author self-archiving of the accepted manuscript version of this article is solely governed by the terms of such publishing agreement and applicable law.

Authors and Affiliations

Halil Dinçer[1,3] · Sadık Can Girgin[2]

✉ Halil Dinçer
halil.dincer@balikesir.edu.tr

[1] The Graduate School of Natural and Applied Sciences, Dokuz Eylül University, Izmir, Türkiye

[2] Department of Civil Engineering, Dokuz Eylül University, Izmir, Türkiye

[3] Department of Civil Engineering, Balıkesir University, Balıkesir, Türkiye